Cardiovascular Research (2008) **78**, 494–504
doi:10.1093/cvr/cvn023

Analyses of a novel *SCN5A* mutation (C1850S): conduction vs. repolarization disorder hypotheses in the Brugada syndrome

Séverine Petitprez[1†], Thomas Jespersen[1†], Etienne Pruvot[2], Dagmar I. Keller[3], Cora Corbaz[2], Jürg Schläpfer[2], Hugues Abriel[1,2*‡], and Jan P. Kucera[4*‡]

[1]*Department of Pharmacology and Toxicology, University of Lausanne, 27, Bugnon, 1005 Lausanne, Vaud, Switzerland;* [2]*Service of Cardiology, CHUV, Lausanne, Switzerland;* [3]*Department of Cardiology, University Hospital, Basel, Switzerland; and* [4]*Department of Physiology, University of Bern, Bühlplatz 5, 3012 Bern, Switzerland*

Received 28 March 2007; revised 28 January 2008; accepted 31 January 2008; online publish-ahead-of-print 5 February 2008

Time for primary review: 29 days

KEYWORDS
Brugada syndrome;
Sodium channel;
Genetics;
Electrophysiology;
Computational analysis

Aims Brugada syndrome (BrS) is characterized by arrhythmias leading to sudden cardiac death. BrS is caused, in part, by mutations in the *SCN5A* gene, which encodes the sodium channel alpha-subunit $Na_v1.5$. Here, we aimed to characterize the biophysical properties and consequences of a novel BrS *SCN5A* mutation.

Methods and results *SCN5A* was screened for mutations in a male patient with type-1 BrS pattern ECG. Wild-type (WT) and mutant $Na_v1.5$ channels were expressed in HEK293 cells. Sodium currents (I_{Na}) were analysed using the whole-cell patch-clamp technique at 37°C. The electrophysiological effects of the mutation were simulated using the Luo-Rudy model, into which the transient outward current (I_{to}) was incorporated. A new mutation (C1850S) was identified in the $Na_v1.5$ C-terminal domain. In HEK293 cells, mutant I_{Na} density was decreased by 62% at −20 mV. Inactivation of mutant I_{Na} was accelerated in a voltage-dependent manner and the steady-state inactivation curve was shifted by 11.6 mV towards negative potentials. No change was observed regarding activation characteristics. Altogether, these biophysical alterations decreased the availability of I_{Na}. In the simulations, the I_{to} density necessary to precipitate repolarization differed minimally between the two genotypes. In contrast, the mutation greatly affected conduction across a structural heterogeneity and precipitated conduction block.

Conclusion Our data confirm that mutations of the C-terminal domain of $Na_v1.5$ alter the inactivation of the channel and support the notion that conduction alterations may play a significant role in the pathogenesis of BrS.

1. Introduction

Brugada syndrome (BrS) is a disorder characterized by ST segment elevation in the right precordial leads V1–V3 on the surface ECG, with atypical right bundle branch block pattern, and an increased risk for sudden cardiac death (SCD).[1] The BrS is a primary electrical cardiac disorder, which is inherited as an autosomal dominant trait. Many mutations in *SCN5A*, encoding the α-subunit of the voltage-gated sodium channel $Na_v1.5$, have been identified,[2] though only 10 to 30% of clinically affected individuals carry a mutation in this gene.[3] Among the ~90 mutations reported thus far,[2] only a few of them have been characterized at the molecular and biophysical level using cellular expression systems.[1] Most of *SCN5A* mutations lead to a 'loss-of-function' by reducing the sodium current (I_{Na}) available during the phases 0 (upstroke) and 1 (early repolarization) of the cardiac action potential (AP).[1] Despite more than 10 years of research in this field, the molecular and cellular mechanisms leading to the BrS are not yet completely understood.[1] Interestingly, in some patients, BrS is concealed on the surface ECG and can be unmasked using sodium channel blockers[4] or during fever episodes.[5]

Here, we screened *SCN5A* in a patient with typical clinical manifestations of BrS. A novel mutation, C1850S, located in the C-terminal domain of $Na_v1.5$ was identified.

* Corresponding author. Tel: +41 21 692 5364; fax: +41 21 692 5355 (H.A); Tel: +41 31 631 87 59; fax: +41 31 631 4611 (J.P.K.).
E-mail addresses: hugues.abriel@unil.ch (H.A.); kucera@pyl.unibe.ch (J.P.K.)
† These authors contributed equally to this study.
‡ These authors share the last authorship of this article.

When mutant channels were expressed in HEK293 cells, the peak I_{Na} density was decreased by 62% (at -20 mV) and fast I_{Na} inactivation was accelerated.

Computer simulations were conducted using the Luo-Rudy (LRd) model to examine the interaction of I_{Na} and the transient outward current (I_{to}), proposed to determine early repolarization in the right epicardium.[6] The I_{to} density necessary to precipitate repolarization was similar in the presence of wild-type (WT) and mutant I_{Na}; however, our computational analyses suggest that conduction in structurally discontinuous tissue is prone to block and much more sensitive to I_{to} in the presence of the mutation at the heterozygous state. Moreover, these manifestations are modulated by the extracellular concentration of K^+. Our data confirm that mutations of the C-terminal domain of $Na_v1.5$ alter the inactivation properties of the channel and support the notion that conduction disturbances may be involved in the pathogenesis of BrS.

2. Methods

2.1 Molecular screening

Genomic DNA was extracted from peripheral lymphocytes, and all coding exons of *SCN5A* were amplified by polymerase chain reaction, using primers designed in intronic flanking sequences according to the gene sequences.[7] Denaturating high performance liquid chromatography (DHPLC) was performed on DNA-amplification products on at least one temperature condition. Abnormal DHPLC profiles were analysed by sequence reaction in both strands of the exon, using Big Dye termination mix, and analysed by cycle sequencing on an automated laser fluorescent DNA sequencer (ABI prism 3100, Applied Biosystems). The novel mutation C1850S was absent in 200 normal alleles. The investigation conformed with the principles outlined in the Declaration of Helsinki. The index patient gave written informed consent to participate in the study.

2.2 Electrophysiology

SCN5A mutation was engineered into WT cDNA (clone hH1a received from Dr R. Kass) cloned in pcDNA3.1 (Invitrogen), using the QuickChange Kit (Stratagene) and verified by sequencing. For electrophysiology studies, HEK293 cells were transiently transfected with 0.6 μg of WT or mutant $Na_v1.5$ construct cDNAs or 0.3 μg of each. All transfections included 2.0 μg pIRES-hβ1-CD8 cDNA encoding hβ1 subunit and CD8 antigen as a reporter gene. Cells were transfected using calcium phosphate or Lipofectamine® and I_{Na} were measured after 48 h. Anti-CD8 beads (Dynal) were used to identify transfected cells. Patch-clamp recordings were conducted using an internal solution containing (mmol/L) CsCl 60; CsAspartate 70; EGTA 11; $MgCl_2$ 1; $CaCl_2$ 1; HEPES 10; and Na_2-ATP 5, pH 7.2 with CsOH; external solution NaCl 130; $CaCl_2$ 2; $MgCl_2$ 1.2; CsCl 5; HEPES 10; and glucose 5, pH 7.4 with CsOH. Using these solutions, 5 min after rupturing the membrane, we observed no significant alteration of the availability curve and the peak current. Peak currents were measured during an inactivation protocol and I_{Na} densities (pA/pF) were obtained by dividing the peak I_{Na} by the cell capacitance obtained from the pClamp function (pClamp suite, v.8, Axon Instruments, CA, USA). For the activation and steady-state inactivation curves, data from individual cells were fitted with Boltzmann relationship, $y(V_m) = 1/\{1 + \exp[(V_m - V_{1/2})/K]\}$, in which y is the normalized current or conductance, V_m is the membrane potential, $V_{1/2}$ is the voltage at which half of the channels are activated or inactivated, and K is the slope factor. Recovery from inactivation curves were fitted individually with a mono-exponential relationship. I_{Na} were measured using a VE-2 amplifier (Alembic Instruments, Montréal, QC) allowing a full compensation of the series resistance, and were analysed using the pClamp software suite. No correction of liquid junction potentials was performed. All measurements were carried out at $37 \pm 1^\circ$C using a control system (Cell MicroControls) heating the perfusion solution.

2.3 Biochemistry

Western blotting conditions have been described previously.[8] The anti-$Na_v1.5$ affinity purified antibody recognizes residues 493–511 of rat $Na_v1.5$ (ASC-005, Alomone). These residues are identical in the human sequence. The anti-actin antibody was from Sigma.

2.4 Statistics

Data are presented as means ± SEM. The two-tailed Student *t*-test or the ANOVA test with the Bonferroni correction were used to compare means; $P < 0.05$ was considered significant.

2.5 Mathematical modelling of I_{Na}, the action potential, and conduction

The LRd model of the ventricular epicardial cell[9] was used to reconstruct I_{Na} under voltage clamp conditions as well as the AP of the epicardial myocyte. The model incorporated the updates published by Faber and Rudy[10] as well as the ATP-sensitive K^+ current as described by Shaw and Rudy.[11] The transient outward K^+ current I_{to} was introduced into the model according to the formulation of Dumaine *et al.*[12] To account for the important heterogeneity of I_{to} expression between the left and right ventricles and across the myocardial wall, simulations were run over a broad range of I_{to} maximal conductance (g_{to}, from 0 to 4 mS/μF).

In the LRd model, I_{Na} is formulated as $I_{Na} = g_{Na} \cdot m^3 hj(V_m - E_{Na})$, where g_{Na} is the maximal conductance of I_{Na} (16 mS/μF), m, h, and j are the activation, fast inactivation, and slow inactivation gating variables, respectively, and E_{Na} is the Na^+ Nernst potential. The effects of the C1850S mutation (CS) were simulated by modifying β_h, (the closing rate of the fast inactivation gate h) in a voltage-dependent manner consistent with our experimental findings to account for (i) the decrease of peak I_{Na} by 62% at $V_m = -20$ mV; (ii) the shift of the $V_{1/2}$ of steady-state inactivation by 11.6 mV towards more negative potentials; and (iii) the voltage-dependent decrease of the time constant of fast I_{Na} inactivation for $V_m \geq -40$ mV.

The WT and CS formulations of β_h are as follows:

WT (Original formulation of the LRd model):

$$\text{For } V_m < -40\,\text{mV}: \beta_{h,WT} = 3.56\exp(0.079V_m) + 3.1 \times 10^5 \exp(0.35V_m).$$

$$\text{For } V_m \geq -40\,\text{mV}: \beta_{h,WT} = 1/(0.13\,(1 + \exp((V_m + 10.66)/(-11.1)))).$$

CS:

$$\text{For } V_m < -40\,\text{mV}: \beta_{h,CS} = 2.8606\,(\exp(0.0672\,(V_m + 40))).$$

$$\text{For } V_m \geq -40\,\text{mV}: \beta_{h,CS} = \beta_{h,WT}(1.5 + 4.1\exp(-(V_m + 40)/16.8)).$$

The opening rate constant α_h of gate h as well as the rates of the m and j gates were not modified. To simulate heterozygote (HZ) cells (or I_{Na} in cells transfected with equal amounts of WT and mutant cDNA), g_{Na} was split into two equal components of 8 mS/μF each corresponding to the two SCN5A alleles ($I_{Na} = I_{Na,WT} + I_{Na,CS}$).

Further details concerning the modelling approach are provided in the Supplementary material online.

Table 1 Biophysical properties of I_{Na} recorded in HEK293 cells transfected with wild-type (WT), C1850S, or $^1/_2$WT and $^1/_2$C1850S cDNA. For the activation and steady-state inactivation curves (*Figure 3A*), data points from individual cells were fitted with Boltzmann relationship, and the $V_{1/2}$ and K values of the different conditions are presented; $^*P < 0.05$, $^{***}P < 0.001$ vs. WT, Bonferroni correction after ANOVA test

	Steady state $V_{1/2}$ inactivation (mV)	Slope factor: K inactivation (mV)	$V_{1/2}$ activation (mV)	Slope factor: K activation (mV)	Time to half recovery from fast inactivation (ms)
WT	-78.6 ± 0.8 ($n = 9$)	6.4 ± 0.4 ($n = 9$)	-36.9 ± 1.4 ($n = 7$)	7.0 ± 0.4 ($n = 7$)	3.4 ± 0.3 ($n = 13$)
C1850S	$-90.2 \pm 0.5^{***}$ ($n = 7$)	5.9 ± 0.4 ($n = 7$)	-35.5 ± 1.3 ($n = 5$)	7.4 ± 0.4 ($n = 5$)	3.8 ± 0.4 ($n = 15$)
$^1/_2$WT + $^1/_2$C1850S	$-83.8 \pm 1.8^*$ ($n = 9$)	6.9 ± 0.3 ($n = 9$)	-33.6 ± 1.3 ($n = 8$)	6.4 ± 0.6 ($n = 8$)	3.5 ± 0.6 ($n = 8$)

3. Results

3.1 Index case

The index case was a 55-year old Caucasian male seen at our cardiology clinic (Lausanne, Switzerland) for investigation of a typical type-1 BrS ECG pattern recorded during cystitis with high fever. However, the ECG remained abnormal after fever (*Figure 1A*). The patient never had syncope or palpitations but his mother died suddenly at age 35. The echocardiography was normal. An electrophysiological study was conducted using two quadripolar leads. Premature ventricular stimulation was performed at cycle length of 600 and 400 ms followed by one and then two premature beats. Ventricular fibrillation was reproducibly inducible at a drive train of 400 ms followed by two premature beats at a coupling interval of 240 and 200 ms, respectively. Sinus rhythm was restored by an external biphasic shock of 120 J. No ajmaline test was performed. An internal cardioverter-defibrillator was implanted.

3.2 Identification and characterization of the *SCN5A* mutation

A heterozygous G to C substitution at position 5549 of *SCN5A* resulted in a C1850S mutation in the C-terminal tail of $Na_v1.5$ (*Figure 1B*). In HEK293 cells transiently transfected with WT and mutant cDNAs, Western blot analyses showed that the level of protein expression of C1850S mutant channels was comparable with that of WT (*Figure 1C*). In contrast, using the patch-clamp technique in the whole-cell configuration, at 37°C, C1850S channels generated I_{Na} with biophysical properties that were clearly different compared with WT currents. First, the peak I_{Na} density mediated by C1850S channels was reduced by $62 \pm 5\%$ at -20 mV (*Figure 1D*). When cells were co-transfected with equal amounts of WT and mutant cDNAs to mimic the heterozygous status of the patient, I_{Na} density was intermediate (*Figure 1D*). Furthermore, as illustrated in *Figure 2A*, C1850S currents were almost completely inactivated 2 ms after the voltage step (arrows), while WT currents were still substantial. This indicates that C1850S I_{Na} inactivated faster compared with WT I_{Na}. *Figure 2B* shows simulated current traces generated by the original I_{Na} formulation of the LRd model (WT) and by the formulation in which the rate of fast inactivation β_h was modified. Acceleration of fast inactivation without modifying other gating kinetics and without modifying I_{Na} conductance resulted in a reduction of peak I_{Na} by 63% (at -20 mV) and almost complete inactivation after 2 ms, similar to the experimental findings.

In HEK293 cells, the $V_{1/2}$ of voltage-dependence of steady-state inactivation of C1850S was shifted towards more negative values by 11.6 mV (*Table 1* and *Figure 3A*). No significant alteration in the activation curve $V_{1/2}$ was observed. When HEK293 cells were transfected with equal amount of WT and mutant cDNA, the shift of the steady-state inactivation curve was intermediate (*Figure 3A* and *Table 1*). In the I_{Na} model, the shift of the steady-state inactivation curve towards more negative potentials without alterations in recovery from fast inactivation (discussed later) was simulated by increasing the fast inactivation rate β_h in a voltage-dependent manner while leaving α_h unchanged (see Methods).

No change in the kinetics of recovery from fast inactivation was seen (*Figure 4A*). In the mathematical model of I_{Na} (*Figure 4B*), modification of the rate β_h did not alter recovery from inactivation.

As illustrated in *Figure 2A*, fast inactivation is accelerated for the currents mediated by mutant channels compared with WT (arrows in *Figure 2A*). Individual inactivating current traces were fitted using a mono-exponential function and the resulting time constants (τ) were plotted as a function of the different voltages (*Figure 4C*). At voltages more negative than 5 mV, the mutant τ values were significantly shorter compared with WT. In *Figure 4D*, the same analysis is presented for the model WT and mutant I_{Na}. The voltage-dependent behaviour of the τ values in the model is comparable with the behaviour observed for the experiments. In transfected HEK293 cells, we also tested the entry into the intermediate inactivated state,[13] but no difference was observed (see Supplementary material online, *Figure S1*).

3.3 Action potential simulations

It has been postulated that the clinical manifestations of BrS are related to the propensity of right epicardial tissue to premature repolarization, which can explain ST-segment elevation in the right precordial leads and phase 2 re-excitation by deeper layers of myocardium.[6] This susceptibility of the right epicardial AP to lose its dome is explained by the predominance of outward currents over inward currents during phase 1 (notch). During this phase, the balance of transmembrane currents is principally determined by the inactivating I_{Na}, the activating L-type Ca^{2+} current, and the rapidly activating transient outward K^+ current, I_{to}. Thus, under conditions of high levels of I_{to} as encountered in the right epicardium, the loss of the depolarizing contribution of I_{Na} caused by its accelerated

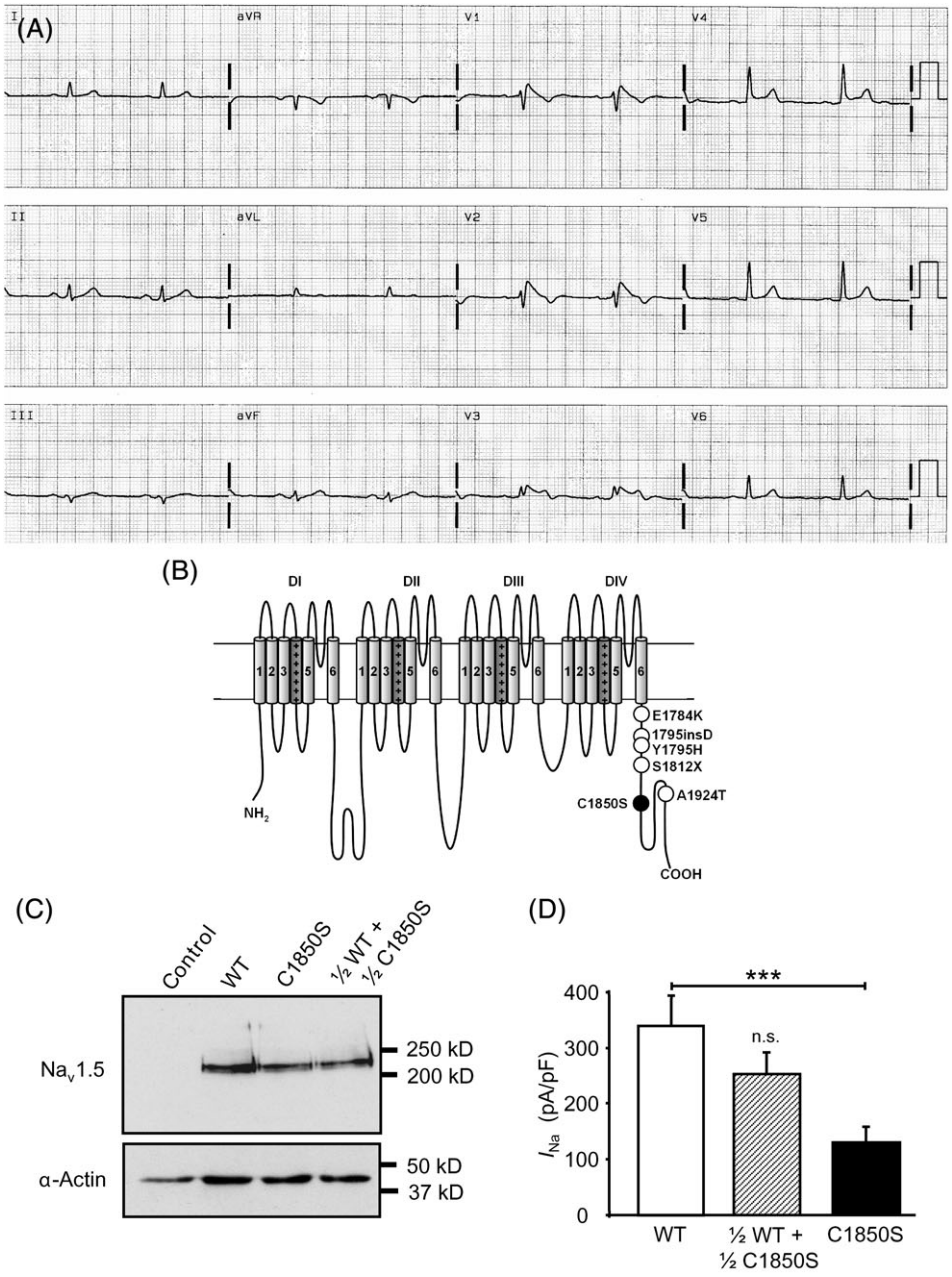

Figure 1 Electrocardiogram of the index case, mutations in $Na_v1.5$ C-terminus, and expression of wild-type (WT) and C1850S $Na_v1.5$ channels. (*A*) ECG of the index case at baseline without fever. (*B*) Membrane topology of $Na_v1.5$. Location of the novel C1850S mutation (black circle) and five BrS mutations located in the C-terminus (white circles). (*C*) Western blot of HEK293 cell lysates expressing WT, C1850S, and 50/50% WT/C1850S channels. Controls are non-transfected cells. (*D*) I_{Na} density at 37°C of HEK293 cells transiently transfected with WT, 50/50% WT/C1850S and C1850S cDNA; $n = 14$, 10, 14 cells, respectively; ***$P < 0.001$. n.s. not significant vs. 50/50% WT/C1850S.

inactivation can promote early repolarization.[14] In addition, it was reported that both hyper- and hypokalemia could precipitate the clinical manifestations of BrS.[15,16]

This background motivated us to investigate the consequences of the C1850S mutation on the epicardial AP as a function of the level of I_{to} expression and of extracellular potassium concentration ($[K^+]_o$). Single cell AP simulations were conducted using the LRd model. For every $[K^+]_o$ tested (2.5 to 12.0 mmol/L in steps of 0.5 mmol/L), we determined the critical value of g_{to} above which the AP loses its dome-shaped plateau and repeated this approach for the WT, HZ, and homozygote C1850S (CS) genotypes. As shown in *Figure 5A*, the critical g_{to} was, as expected, the largest for the WT, the smallest for the CS and intermediate for the HZ over the entire range of $[K^+]_o$ tested. Interestingly, there was a biphasic dependence of critical g_{to} on $[K^+]_o$ for all three genotypes with a maximum near $[K^+]_o = 6$ mmol/L. *Figure 5B* illustrates this loss of the AP dome with increasing levels of I_{to} at a normal $[K^+]_o$ of 4 mmol/L. Increasing g_{to} led first to a loss of the dome in the CS (b), then in the HZ (c) and finally in the WT (d). Thus, accelerated inactivation of I_{Na} may lead to premature epicardial repolarization under conditions of elevated I_{to} expression, which, *in vivo*, can be encountered in the right ventricular epicardium.[17] However, the critical g_{to} values

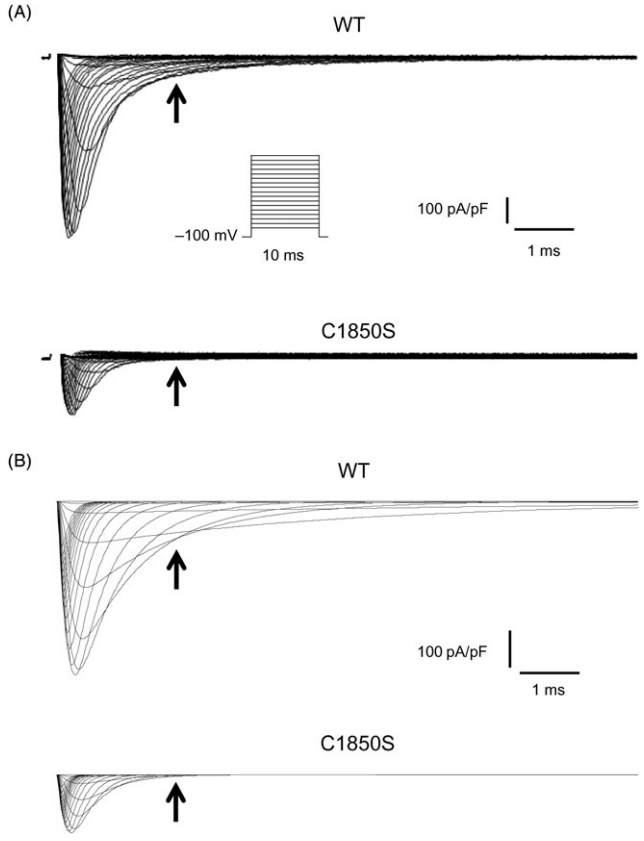

Figure 2 Wild-type (WT) and C1850S currents recorded in HEK293 cells and their simulations. (*A*) Current traces recorded at 37°C from cells expressing WT or C1850S channels in response to a series of 10-ms pulses (inset). Arrows at 2 ms after onset of the voltage-step indicate the faster inactivation of C1850S I_{Na} compared with WT. The fast transient capacitive current is blanked for sake of clarity. (*B*) Reconstruction of WT and C1850S currents using the original I_{Na} of the Luo-Rudy model (WT) and the I_{Na} model in which β_h was modified (see 'Methods').

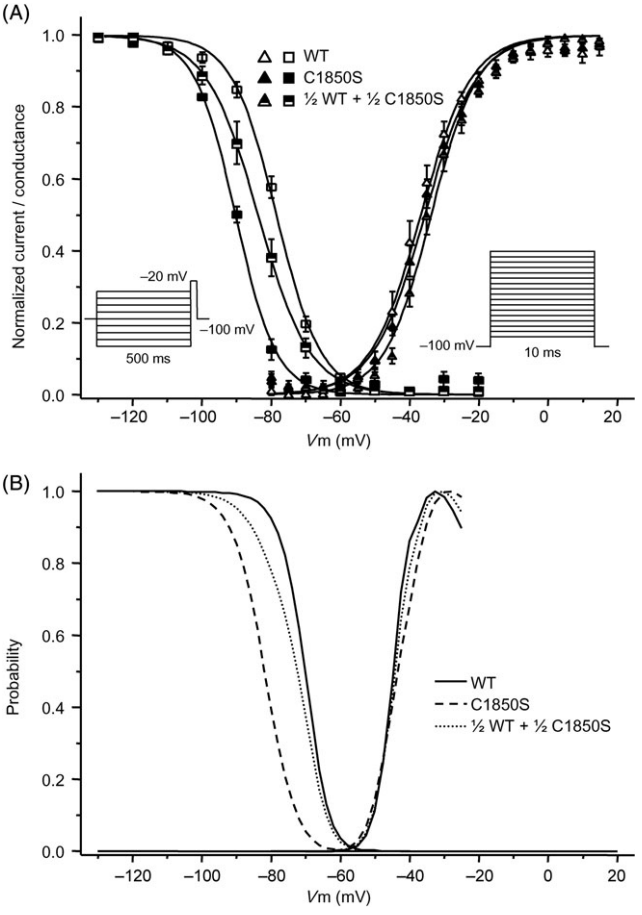

Figure 3 Voltage-dependence of activation and inactivation. (*A*) Activation (triangles) and inactivation (squares) curves at 37°C. Activation properties were determined from I/V relationships (obtained after applying the step protocol in inset) by normalizing peak I_{Na} to driving force and maximal I_{Na}, and plotting normalized conductance vs. V_m. Voltage-dependence of steady-state inactivation was obtained by plotting the normalized peak current (25-ms test pulse to −20 mV after a 500-ms conditioning pulse, see inserted protocol) vs. V_m. Boltzmann curves were fitted to both activation and steady-state inactivation data. Averaged values and the number of cells used are presented in *Table 1*. (*B*) Steady-state activation and inactivation curves of the model I_{Na}. These curves were generated using exactly the same voltage-clamp protocols and analyses as in the experiments.

differed only by a few percent between WT and CS, and the difference between WT and HZ conditions was <1% for all values of $[K^+]_o$.

It is well known that the clinical manifestations of BrS are rate-dependent.[18] Moreover, AP characteristics during pacing at a physiological rate differ from those of an isolated AP elicited in a resting cell. Therefore, to evaluate the behaviour of the model cell paced at a physiological rate, we conducted simulations in which trains of stimuli were applied during 30 s following the initial 1-min period without pacing. *Figure 5C* compares APs in the simulated WT, HZ and C1850S mutant cells during 30 s of pacing at a rate of 1 Hz, for $[K^+]_o$ = 4 mmol/L and with g_{to} = 1.315 mS/μF. This value of g_{to} was inferior to the thresholds at which premature repolarization occurred for the isolated AP (see *Figure 5A*). While no premature repolarization occurred during the entire train in the WT cell, premature repolarization occurred for the second last AP of the train in the HZ cell (asterisk). In the C1850S cell, premature repolarization occurred earlier in the train. When g_{to} was substantially increased (>1.5 mS/μF, not shown), the APs exhibited an irregular sequence of spike and dome and premature repolarization morphologies for all three genotypes and the average rate at which premature repolarization occurred was not manifestly different.

We then extended the investigation of the critical g_{to} level leading to premature repolarization to the situation of the paced cell. The critical level was defined as the boundary between the complete absence of premature repolarization during the 30-s train and the presence of at least one AP exhibiting premature repolarization. These simulations were conducted at pacing rates of 1 and 2 Hz (*Figure 5D* and *E*, respectively). For all three genotypes, the boundaries exhibited a similar shape as in the single AP simulations but were shifted towards smaller values of g_{to}. This shift was more prominent at 2 Hz than at 1 Hz. Nevertheless, for both pacing rates and for all values of $[K^+]_o$, the critical g_{to} values differed only by a few percent (<1% between WT and HZ), similar to the single AP simulations.

3.4 The C1850S mutation causes conduction block in branching tissue

It has recently been proposed that right ventricular fibrosis may contribute to the genesis of conduction disorders

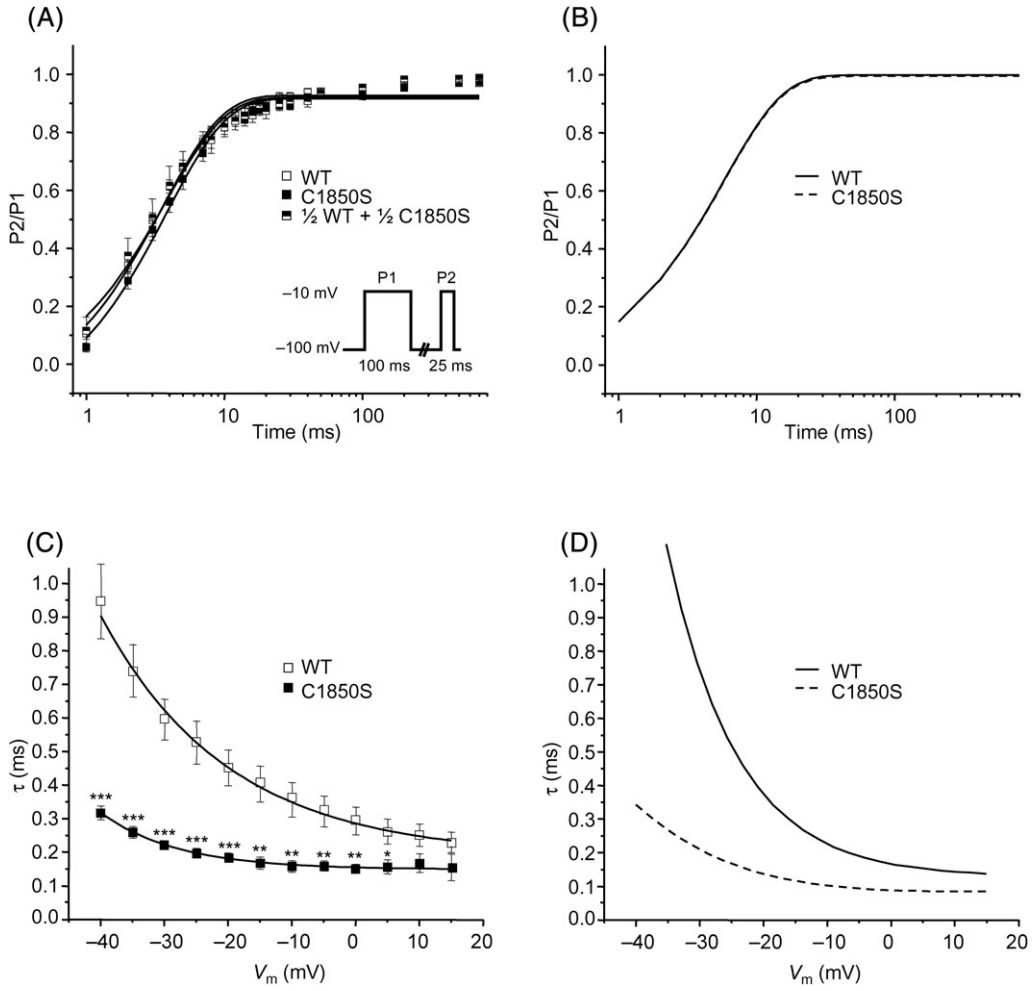

Figure 4 Recovery from inactivation and onset of inactivation. (*A*) Recovery from inactivation recorded at 37°C (protocol in inset) was characterized by the time to half recovery (*Table 1*). Data were fitted using mono-exponential functions (solid lines). Averaged values and the number of cells used are presented in *Table 1*. (*B*) Simulated recovery from inactivation, using the same protocol as in *A*. (*C*) Onset of inactivation is accelerated for C1850S at 37°C. τ values were obtained by fitting the decaying phase of individual current traces (*Figure 2A*) with a mono-exponential function and plotted vs. V_m; $n = 7$ and 5 cells for WT and C1850S, respectively; $^*P < 0.05$, $^{**}P < 0.01$, $^{***}P < 0.001$. (*D*) Corresponding values of τ for the simulated I_{Na}. These values were obtained using the same protocols and analyses as in *C*.

leading to the characteristic BrS ECG.[19,20] Fibrous cardiac tissue is characterized by sparsely connected strands and sheets of myocardium intermingled with unexcitable tissue (*Figure 6A*), and such structures are known to form the substrate of slow conduction or conduction block.[21]

Therefore, we investigated the consequences of the C1850S mutation on conduction characteristics along a 121-cell strand releasing two branches from its centre (*Figure 6A*). These simulations were conducted for a single AP. In the simulation presented in *Figure 6B*, the branches were 20 myocytes long. This branch length was several times the space constant of the strand, which amounted to 533 μm (approximately five cells) at $[K^+]_o = 4$ mmol/L (the space constant was not influenced by g_{to} or by the I_{Na} genotype). This simulation corresponds to scarce lateral coupling between fibres. The branching strand was characterized by a mismatch between the current generated by the strand before the branch point and the increased load represented by the distal segment of the strand and the two branches.[22]

Figure 6B shows AP upstrokes, WT and mutant I_{Na} currents as well as I_{to} in the vicinity of the branch point for both the WT and the HZ ($g_{to} = 0.5$ mS/μF, $[K^+]_o = 4$ mmol/L). In the WT, the current-to-load mismatch resulted in slow upstrokes and a local conduction delay (0.92 ms). In the HZ, the reduced total I_{Na} shifted the current-to-load balance in favour of the load, which resulted in conduction block.

In *Figure 6C*, the dependence of the conduction delay and the occurrence of block were investigated as a function of g_{to} in strands releasing branches of different lengths (20, 10, 7, 5, and 2 myocytes).

In the absence of I_{to} ($g_{to} = 0$), conduction was successful for both genotypes but, irrespective of branch length, the conduction delay for the HZ was always longer than for the WT. For branch lengths of 20, 10, 7 and 5 myocytes, increasing g_{to} led to a progressively increasing conduction delay, until conduction block occurred. The prolongation of the conduction delay was much more prominent for the HZ and the level of g_{to} at which block occurred was considerably lower. While, for both genotypes, the g_{to} level at which block occurred was almost the same for branch lengths of 20 and 10 myocytes, this g_{to} level was larger for shorter branches. Only when branches were much shorter (two

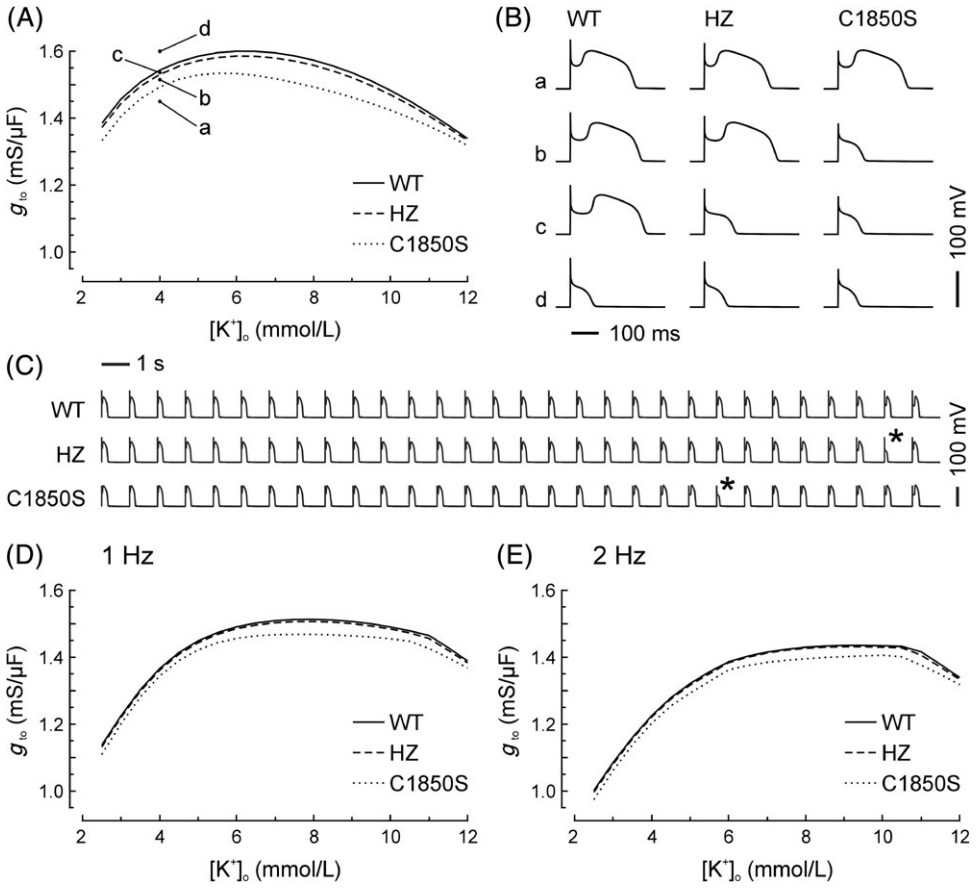

Figure 5 Investigation of the action potential (AP) phenotype in single cell simulations. (*A*) Boundaries between the spike and dome and premature repolarization phenotypes in the ($[K^+]_o$, g_{to}) parameter space for the WT, HZ and C1850S genotypes. Combinations of $[K^+]_o$ and g_{to} below the corresponding curves produce a spike and dome phenotype and combinations above the curves lead to loss of the dome and premature repolarization. The points labelled a–d correspond to the APs shown in *B*. (*B*) APs for the three genotypes at a constant $[K^+]_o$ (4 mmol/L) but at increasing levels of g_{to}. a: g_{to} = 1.450 mS/μF; b: g_{to} = 1.515 mS/μF; c: g_{to} = 1.535 mS/μF; d: g_{to} = 1.600 mS/μF. (*C*) Trains of 30 APs elicited at 1 Hz following a resting period of 1 min, for the three genotypes. $[K^+]_o$ = 4 mmol/L and g_{to} = 1.315 mS/μF. Asterisks indicate premature repolarization. (*D*) Boundaries between the spike and dome and premature repolarization phenotypes in the ($[K^+]_o$, g_{to}) parameter space for the three genotypes, for trains of 30 action potentials elicited at 1 Hz. Combinations of $[K^+]_o$ and g_{to} above the corresponding curves lead to loss of the dome and premature repolarization in at least one AP. (*E*) Same as *D*, but for trains of 60 APs elicited at 2 Hz.

cells) than the space constant, conduction did not fail and the conduction delay remained small for both the WT and the HZ.

Thus, successful conduction in the branched HZ strand is strongly dependent on I_{to} and branch length. This contrasts with the minimal dependence of the velocity of continuous conduction on I_{to}: as illustrated in *Figure 6D*, increasing g_{to} from 0 to 4 mS/μF slowed conduction by a few percent only.

When the local conduction delay across the branch point was longer than ∼1 ms, it provided enough time for I_{to} to activate in the cells immediately before the branch point. The activated I_{to} then acted to diminish the amount of current available to depolarize the cells beyond the branch point to threshold. When g_{to} was increased, it therefore resulted in a prolongation of the conduction delay and precipitated block. In the presence of mutant I_{Na} characterized by accelerated inactivation, the marked diminution of I_{Na} after 1–2 ms (*Figure 2*) further exacerbated these alterations of conduction.

In *Figure 6E*, the (g_{to},$[K^+]_o$) parameter space was explored to identify the combinations of g_{to} and $[K^+]_o$ leading to conduction block in the HZ but not in the WT (light grey area). In this series of simulations, branches were 20 myocytes long. $[K^+]_o$ was varied from 2.5 to 12.0 mmol/L in steps of 0.5 mmol/L, and, for each tested $[K^+]_o$, the critical value of g_{to} at which conduction block occurred was assessed with a precision of 0.005 mS/μF. Conduction block in the HZ but not in the WT was obtained in a wide region in the parameter space, delimited by bell-shaped boundaries. Furthermore, for all $[K^+]_o$, there was a several fold difference between WT and HZ regarding the critical levels of g_{to} at which block occurred. A qualitatively similar difference was observed for branches 10, 7, and 5 myocytes long (data not shown). These findings therefore suggest that in discontinuous cardiac tissue, mutations of I_{Na} exhibiting biophysical characteristics similar to those of the C1850S mutant result in cardiac excitation that is definitely more prone to slow conduction and conduction block, the key ingredients of re-entrant arrhythmogenesis.[21]

4. Discussion

In this study, we investigated the biophysical characteristics of a novel *SCN5A* BrS mutation, C1850S, at physiological temperature. In addition, we performed AP and conduction simulations using the LRd model to investigate the

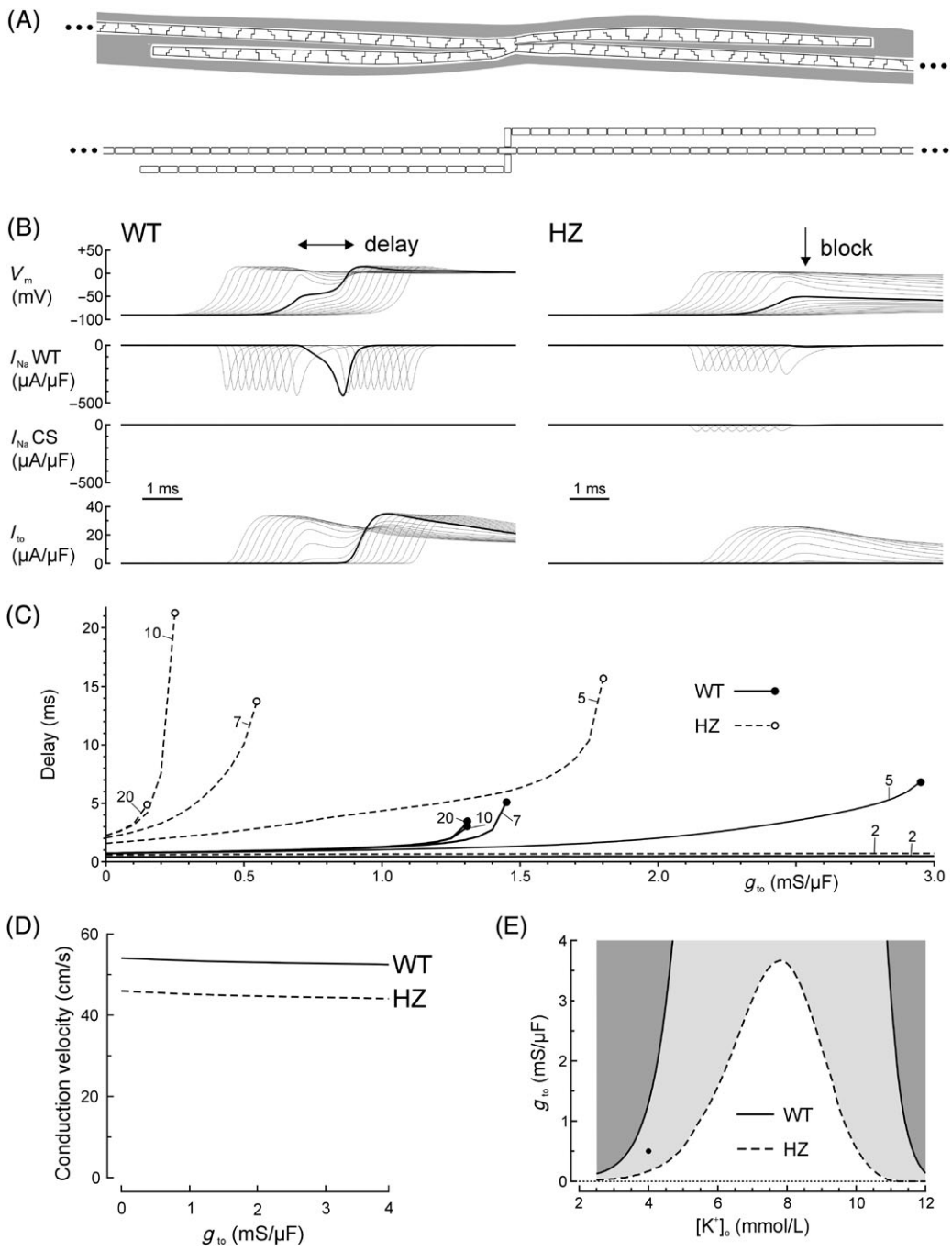

Figure 6 Conduction in a discontinuous structure is more prone to block in the presence of the C1850S mutation. (*A*) Schematic of discontinuous cardiac tissue (top) and its representation using the Luo-Rudy model as a strand releasing two branches (bottom). Gray areas represent inexcitable clefts (e.g. connective tissue in fibrosis) between scarcely connected parallel fibres of cardiac myocytes. (*B*) Simulated action potentials (V_m), WT and mutant I_{Na} as well as I_{to} for the wild-type (WT) and heterozygote (HZ) genotypes. Branches were 20 myocytes long in this simulation. Data are shown for the 10 cells proximal and distal to the branch point. The bold traces correspond to the cell at the branch point. $g_{to} = 0.5$ mS/μF and $[K^+]_o = 4$ mmol/L. (*C*) Conduction delay across the branch point for $[K^+]_o = 4$ mmol/L, as a function of g_{to} for the WT and HZ genotypes. These simulations were conducted with branches 20, 10, 7, 5, and 2 myocytes long (labels). Round symbols denote the occurrence of conduction block. (*D*) Conduction velocity in unbranched WT and HZ strands as a function of g_{to} ($[K^+]_o = 4$ mmol/L). (*E*) Boundaries between successful conduction and conduction block in the ($[K^+]_o$, g_{to}) parameter space for the WT and HZ genotypes (branch length: 20 cells). Combinations of $[K^+]_o$ and g_{to} above the corresponding curves lead to conduction block (white area: successful conduction for both genotypes; light grey area: successful conduction for the WT genotype but block for the HZ genotype; dark grey area: conduction block for both genotypes). The dot corresponds to the simulation represented in *B*.

mechanisms underlying the arrhythmogenic alterations of repolarization and conduction. C1850S channels generated smaller peak I_{Na}, and many of the $Na_v1.5$ steady-state and time-dependent inactivation properties were altered. These alterations significantly reduce I_{Na} during the early phases of the AP. The simulations suggest that at the heterozygous state, the mutation can depress conduction in myocardium exhibiting sites of current-to-load mismatch, as exemplified in our study by a myocyte strand releasing branches.

4.1 Heterogeneity of the biophysical properties of Brugada syndrome $Na_v1.5$ channels

Thus far, the cardiac arrhythmias database[2] of the European Society of Cardiology lists more than 90 *SCN5A* BrS mutations. Among them, five are located in the intracellular C-terminus of $Na_v1.5$ (*Figure 1B*). Functional characterization has been performed for only 23 mutations (three of them are in the C-terminus).[23] The vast majority of these mutations reduce the I_{Na} mediated by $Na_v1.5$. However, the molecular mechanisms underlying this reduction are very heterogeneous,[23] and most of the mutant channels have a unique pattern of alterations. One can divide these mechanisms into (1) alterations leading to a reduced I_{Na} membrane density, and (2) changes in biophysical properties.[23] The mutation found in this BrS patient replaces Cys-1850 by a Ser located in a highly conserved part of the C-terminus of $Na_v1.5$. It appears that the first 150 residues of the C-terminus form a highly structured domain comprising six α-helices.[24] Without more knowledge about the detailed role of this domain, one cannot but speculate about the consequences of this mutation. The biophysical alterations induced by C1850S are mainly related to the I_{Na} fast inactivation process. The negative shift of the steady-state availability curve and faster onset of fast inactivation are both consistent with a 'stabilization' of inactivated states (fast and slow/intermediate) of mutant channels. Altogether, these findings suggest that Ser-1850, by enhancing the inactivation process, contributes to a 'loss-of-function' of mutant channels. Our simulations suggest that acceleration of inactivation alone (determined by the rate β_h) can underlie both the acceleration of inactivation and the shift of steady-state inactivation (by rendering inactivated states more stable) without influencing the activation process.

4.2 Action potential and conduction alterations in the Brugada syndrome

The molecular, cellular, and arrhythmogenic mechanisms underlying the ECG alterations seen in BrS are still a matter of debate.[1] According to the 'repolarization disorder hypothesis', re-entrant arrhythmias are caused by a heterogeneous loss of the AP epicardial dome leading to epicardial dispersion of refractoriness, which forms the substrate for reentry. According to the 'conduction disorder hypothesis', the typical ECG signs can be explained by slow conduction and activation delays in the right ventricle (in particular in the right ventricular outflow tract).

Our computational results support the conduction disorder hypothesis. On the one hand, loss of the dome was more prone to occur in the presence of mutant I_{Na} in single cells. However, the level of I_{to} at which abrupt repolarization occurred was only minimally smaller (1%) for the HZ compared with the WT. On the other hand, in discontinuous tissue, conduction delays and block were markedly potentiated by the presence of mutant I_{Na}. Interestingly, the levels of I_{to} conductance at which these manifestations occurred were strikingly different from those necessary to result in premature repolarization. Increasing g_{to} to 1.3 mS/μF or more was necessary to result in a loss of the dome in the HZ cell. However, in the branched HZ tissue, a prominent prolongation of the branching-induced local conduction delay and conduction block were already observed at g_{to} levels <0.6 mS/μF for branches consisting of five myocytes or more. In the original formulation of right ventricular I_{to} by Dumaine *et al.*,[12] a value of 1.1 mS/μF was used. In human right ventricular tissue,[17] maximal peak I_{to} was measured to be 9.8 pA/pF (at $+60$ mV at 36°C), which translates, assuming a reversal potential of -90 mV and a maximal channel open probability of 0.25, to $\sim$0.25 mS/μF. Our study thus suggests that I_{to}-mediated premature repolarization would require a considerable increase in I_{to} density, while conduction alterations in discontinuous tissue could occur at I_{to} levels comparable with those measured previously. In view of the recent findings indicating that structural abnormalities may be involved in the pathogenesis of BrS,[19,20] we therefore propose the 'conduction disorder in discontinuous tissue hypothesis' as a further mechanism that should deserve a particular attention.

4.3 Role of I_{to} in discontinuous conduction

It has been shown[21] that the L-type calcium current ($I_{Ca,L}$) greatly contributes to the success of conduction when conduction is characterized by local conduction delays that extend beyond I_{Na} inactivation. In such situations, suppression of $I_{Ca,L}$ can precipitate conduction block. Because the time to peak of $I_{Ca,L}$ and I_{to} is very similar, our study indicates that I_{to} modulates discontinuous conduction via an analogous mechanism with an opposed polarity. Thus, an increased I_{to} density may precipitate block across a discontinuous structure, while blocking I_{to} may result in a recovery from conduction block. Moreover, our 'conduction disorder in discontinuous tissue' concept is in line with the recent finding that a BrS ECG pattern can also be caused by mutations causing loss of function of $I_{Ca,L}$.[25]

4.4 Effects of extracellular $[K^+]$

Previous work has shown that both hypo- and hyperkalemia can exacerbate the ECG phenotype of BrS.[15,16] In our simulations, we observed a biphasic dependence on $[K^+]_o$ of the level of g_{to} leading to conduction block in the branching strand (*Figure 6E*). This biphasic dependence is reminiscent of the well-known biphasic dependence of conduction velocity (CV) on $[K^+]_o$, which was investigated computationally in detail by Shaw and Rudy.[26] As shown in their work, when the resting membrane is hyperpolarized by a decrease of $[K^+]_o$, CV decreases because the charge necessary to bring the membrane to threshold increases. However, during elevation of $[K^+]_o$, CV initially increases (supernormal conduction) until K^+-induced membrane depolarization results in an increasing fraction of inactivated I_{Na}, leading then to conduction slowing. In the setting of a current-to-load mismatch, as exemplified by tissue branching, this consideration regarding the charge necessary to reach threshold (load) vs. the available I_{Na} also explains the biphasic behaviour of conduction block in the branching strand. Thus, our results are in agreement with the notion that changes in $[K^+]_o$ in both directions may exacerbate the clinical manifestations of carriers of mutations leading to a loss of I_{Na} function. Moreover, it could be hypothesized that, among other factors, variations in plasma $[K^+]_o$ may play a role in the transient nature of the BrS ECGs.

4.5 Study limitations

The clinical manifestations of BrS are rate-dependent.[18] Because of the computational cost of the LRd model, we did not investigate the rate-dependence of conduction characteristics in the branching strands and left the rate-dependent aspects of BrS during long term pacing of single cells out of our study. The simulations of conduction therefore suffer from the limitation that a single stimulus was applied instead of continuous pacing until intracellular ion concentrations have reached their true steady state. As shown in this study, the AP phenotype and conduction block in discontinuous tissue critically depend on the balance between inward and outward currents during early repolarization. Furthermore, the rate-dependence of the AP and of conduction is governed by very intricate dynamic interactions between repolarization, recovery of I_{Na} from inactivation and intracellular Na^+ and Ca^{2+} overload at rapid pacing rates.[10,27] Pacing at different rates or during different periods of time will therefore affect the availability of I_{Na}, $I_{Ca,L}$, and I_{to} during the early phases of the AP and thus the quantitative outcome of the simulations in comparison to an isolated stimulus.

Because numerous membrane transporters relevant to Na^+ and K^+ homeostasis are not incorporated into the LRd model (e.g. the Na^+/glucose symport and the Na^+/H^+ exchanger), it cannot be absolutely guaranteed that the intracellular ion concentrations in the model exactly match those in the human heart *in vivo*. One can nevertheless speculate that at a given heart rate, $[Na^+]_i$ might be lower in the presence of the mutation because less Na^+ enters the cell during the AP upstroke. This would increase the driving force for I_{Na}. While this increase might partially compensate for the I_{Na} loss due to the mutation, it appears however unlikely that the extent of this increase would suffice to fully offset the loss of I_{Na} that we observed experimentally.

In addition, since the patient also showed a BrS ECG at normal temperature, we did not test for effects of higher temperature on the biophysical characteristics of mutant cells.

4.6 Conclusions

In conclusion, these results confirm that mutations of the C-terminal domain of $Na_v1.5$ significantly alter the inactivation properties of the channel, and support the notion that conduction alterations in discontinuous tissue may be involved in the pathogenesis of BrS. Finally, the computational analyses allowed us to formulate clinically-relevant hypotheses regarding the cellular basis of arrhythmogenesis in the context of BrS, which deserve further investigations.

Supplementary material

Supplementary material is available at *Cardiovascular Research* online.

Conflict of interest: none declared.

Funding

Supported by grants of the Swiss National Science Foundation (PP00-110638/1 to HA and 3100A0-100285 to J.P.K.), CardioMet Center, Fondations Vaudoise de Cardiologie, Rita et Richard Barmé, Carlsberg Foundation to T.J., and Swiss Heart Foundation and L.&Th. La Roche Foundation (Basel) to D.K.

References

1. Meregalli PG, Wilde AA, Tan HL. Pathophysiological mechanisms of Brugada syndrome: depolarization disorder, repolarization disorder, or more? *Cardiovasc Res* 2005;**67**:367–378.
2. Study group on molecular basis of arrhythmias. Inherited Arrhythmias Database http://www.fsm.it/cardmoc/
3. Wilde AA, Antzelevitch C, Borggrefe M, Brugada J, Brugada R, Brugada P *et al*. Proposed diagnostic criteria for the Brugada syndrome: consensus report. *Circulation* 2002;**106**:2514–2519.
4. Priori SG, Napolitano C, Schwartz PJ, Bloise R, Crotti L, Ronchetti E. The elusive link between LQT3 and Brugada syndrome: the role of flecainide challenge. *Circulation* 2000;**102**:945–947.
5. Keller DI, Rougier JS, Kucera JP, Benammar N, Fressart V, Guicheney P *et al*. Brugada syndrome and fever: genetic and molecular characterization of patients carrying SCN5A mutations. *Cardiovasc Res* 2005;**67**:510–519.
6. Antzelevitch C, Brugada P, Brugada J, Brugada R, Shimizu W, Gussak I *et al*. Brugada syndrome: a decade of progress. *Circ Res* 2002;**91**:1114–1118.
7. Wang Q, Li Z, Shen J, Keating MT. Genomic organization of the human SCN5A gene encoding the cardiac sodium channel. *Genomics* 1996;**34**:9–16.
8. van Bemmelen MX, Rougier J-S, Gavillet B, Apotheloz F, Daidie D, Tateyama M *et al*. Cardiac voltage-gated sodium channel $Na_v1.5$ is regulated by Nedd4-2 mediated ubiquitination. *Circ Res* 2004;**95**:284–291.
9. Luo CH, Rudy Y. A dynamic model of the cardiac ventricular action potential. I. Simulations of ionic currents and concentration changes. *Circ Res* 1994;**74**:1071–1096.
10. Faber GM, Rudy Y. Action potential and contractility changes in $[Na^+]_i$ overloaded cardiac myocytes: a simulation study. *Biophys J* 2000;**78**:2392–2404.
11. Shaw RM, Rudy Y. Ionic mechanisms of propagation in cardiac tissue. Roles of the sodium and L-type calcium currents during reduced excitability and decreased gap junction coupling. *Circ Res* 1997;**81**:727–741.
12. Dumaine R, Towbin JA, Brugada P, Vatta M, Nesterenko DV, Nesterenko VV *et al*. Ionic mechanisms responsible for the electrocardiographic phenotype of the Brugada syndrome are temperature dependent. *Circ Res* 1999;**85**:803–809.
13. Wang DW, Makita N, Kitabatake A, Balser JR, George AL Jr. Enhanced Na^+ channel intermediate inactivation in Brugada syndrome. *Circ Res* 2000;**87**:E37–E43.
14. Yan GX, Antzelevitch C. Cellular basis for the Brugada syndrome and other mechanisms of arrhythmogenesis associated with ST-segment elevation. *Circulation* 1999;**100**:1660–1666.
15. Littmann L, Monroe MH, Taylor L III, Brearley J. The hyperkalemic Brugada sign. *J Electrocardiol* 2007;**40**:53–59.
16. Araki T, Konno T, Itoh H, Ino H, Shimizu M. Brugada syndrome with ventricular tachycardia and fibrillation related to hypokalemia. *Circ J* 2003;**67**:93–95.
17. Li GR, Feng J, Yue L, Carrier M. Transmural heterogeneity of action potentials and Ito1 in myocytes isolated from the human right ventricle. *Am J Physiol Heart Circ Physiol* 1998;**275**:H369–H377.
18. Extramiana F, Seitz J, Maison-Blanche P, Badilini F, Haggui A, Takatsuki S *et al*. Quantitative assessment of ST segment elevation in Brugada patients. *Heart Rhythm* 2006;**3**:1175–1181.
19. Coronel R, Casini S, Koopmann TT, Wilms-Schopman FJG, Verkerk AO, de Groot JR *et al*. Right ventricular fibrosis and conduction delay in a patient with clinical signs of Brugada syndrome: a combined electrophysiological, genetic, histopathologic, and computational study. *Circulation* 2005;**112**:2769–2777.
20. Frustaci A, Priori SG, Pieroni M, Chimenti C, Napolitano C, Rivolta I *et al*. Cardiac histological substrate in patients with clinical phenotype of Brugada syndrome. *Circulation* 2005;**112**:3680–3687.
21. Kléber AG, Rudy Y. Basic mechanisms of cardiac impulse propagation and associated arrhythmias. *Physiol Rev* 2004;**84**:431–488.
22. Kucera JP, Rudy Y. Mechanistic insights into very slow conduction in branching cardiac tissue: a model study. *Circ Res* 2001;**89**:799–806.

23. Tan H. Biophysical analysis of mutant sodium channels in Brugada syndrome. In: Antzelevitch C, Brugada P, Brugada J, Brugada R ed. *The Brugada syndrome: From Bench to Bedside*. 1st ed. Blackwell Publishing; 2005. p26–41.
24. Cormier JW, Rivolta I, Tateyama M, Yang AS, Kass RS. Secondary structure of the human cardiac Na^+ channel C terminus: evidence for a role of helical structures in modulation of channel inactivation. *J Biol Chem* 2002;**277**:9233–9241.
25. Antzelevitch C, Pollevick GD, Cordeiro JM, Casis O, Sanguinetti MC, Aizawa Y *et al*. Loss-of-function mutations in the cardiac calcium channel underlie a new clinical entity characterized by ST-segment elevation, short QT intervals, and sudden cardiac death. *Circulation* 2007;**115**:442–449.
26. Shaw RM, Rudy Y. Electrophysiologic effects of acute myocardial ischemia: a mechanistic investigation of action potential conduction and conduction failure. *Circ Res* 1997;**80**:124–138.
27. Kondratyev AA, Ponard JG, Munteanu A, Rohr S, Kucera JP. Dynamic changes of cardiac conduction during rapid pacing. *Am J Physiol Heart Circ Physiol* 2006;**292**:H1796–H1811.